Distribution Agreement

In presenting this thesis as a partial fulfillment of the requirements for a degree from Emory University, I hereby grant to Emory University and its agents the non-exclusive license to archive, make accessible, and display my thesis in whole or in part in all forms of media, now or hereafter now, including display on the World Wide Web. I understand that I may select some access restrictions as part of the online submission of this thesis. I retain all ownership rights to the copyright of the thesis. I also retain the right to use in future works (such as articles or books) all or part of this thesis.

Rachel Lee   November 30th, 2024

Can't Stop the Cleaving: Effects of Mutations in SARS-CoV-2 M^{pro} on Activity and Drug Efficacy

by

Rachel Lee

Stefan Sarafianos
Advisor

Department of Biology

Stefan Sarafianos

Advisor

Megan Cole

Committee Member

Vincent Conticello

Committee Member

2024

Can't Stop the Cleaving: Effects of Mutations in SARS-CoV-2 M^{pro} on Activity and Drug Efficacy

By

Rachel Lee

Stefan Sarafianos
Advisor

An abstract of
a thesis submitted to the Faculty of Emory College of Arts and Sciences
of Emory University in partial fulfillment
of the requirements of the degree of
Bachelor of Science with Honors

Department of Biology

2024

Abstract

Can't Stop the Cleaving: Effects of Mutations in SARS-CoV-2 M^{pro} on Activity and Drug Efficacy
By Rachel Lee

Severe acute respiratory syndrome coronavirus 2 (SARS-CoV-2) is the causative agent of the Coronavirus Disease 2019 (COVID-19) pandemic, which has costed millions of lives globally. The main protease (M^{pro}) of SARS-CoV-2 is a potential drug target for COVID-19 treatments due to its critical role in the SARS-CoV-2 infectious cycle and dissimilarity to human proteases, and it is the target of Paxlovid, a Pfizer antiviral that includes the M^{pro} inhibitor nirmatrelvir (NIR). The E166V mutation in M^{pro} was found in patients with repeated and prolonged treatment with Paxlovid. E166V results in high NIR resistance but comes with a fitness cost due to distortion of the active site and loss of dimerization, which is necessary for proteolytic activity. The L141T mutation was identified in SARS-CoV to stabilize the active site of the enzyme and increase activity. I hypothesize that introduction of the L141T mutation would increase dimerization and thus the enzymatic activity of the Omicron (BA.1) E166V M^{pro} without decreasing NIR resistance. Using a FRET-based activity assay, I determined that the L141T/E166V shows slightly decreased activity and NIR resistance compared to E166V. Using SEC-MALS, I demonstrated that the L141T mutation rescues dimerization in solution from the E166V, indicating that increasing dimerization does not automatically improve activity. In addition, we observed substrate inhibition kinetics in the BA.1 E166V M^{pro}, which has not been previously characterized.

Can't Stop the Cleaving: Effects of Mutations in SARS-CoV-2 M^{pro} on Activity and Drug Efficacy

By

Rachel Lee

Stefan Sarafianos
Advisor

A thesis submitted to the Faculty of Emory College of Arts and Sciences
of Emory University in partial fulfillment
of the requirements of the degree of
Bachelor of Science with Honors

Department of Biology

2024

Acknowledgements

I would like to thank my research mentor Grace Neilsen, who helped to design and advise me during this project. I would like to thank my advisor, Dr. Stefan Sarafianos and the members of the Sarafianos Lab, who have offered their support and knowledge throughout this project. Lastly, thank you to my committee members Dr. Megan Cole and Dr. Vincent Conticello, who have supported me as a student and researcher throughout my time at Emory.

Table of Contents

Illustrations

Figures

Tables

Introduction

Severe acute respiratory syndrome coronavirus 2 (SARS-CoV-2) is the causative agent of

Coronavirus Disease 2019 (COVID-19). As of February 25th, 2024, the COVID-19 pandemic has

resulted in over 774 million cases and over 7 million deaths worldwide ("COVID-19 Cases",

2024). Coronaviruses are a family of enveloped, positive-sense, single-stranded RNA viruses

that can cause mild to severe respiratory disease and include SARS-CoV and MERS-CoV (Hu et

al., 2021, V'kovski et al., 2021). In response to the COVID-19 pandemic, Pfizer developed

Paxlovid, which is an oral antiviral treatment that consists of two tablets, nirmatrelvir (NIR) and

ritonavir, and which has become the leading antiviral against SARS-CoV-2 ("COVID-19

Treatments", 2023).

The main protease (M^{pro}), also called 3C-like protease ($3CL^{pro}$) or non-structural protein 5

(nsp5), of SARS-CoV-2 is a potential drug target for COVID-19 treatments due to its critical role

in the SARS-CoV-2 infectious cycle and its dissimilarity to human proteases (Citarella et al.,

2021, Goyal & Goyal, 2020). M^{pro} performs 11 essential cleavages of the polyprotein 1a/1ab

from non-structural protein 4 (nsp4) to 16 mature nsps, which, among other functions, form the

replication complex that transcribes sub-genomic RNAs for translation by the host and full viral

genomes to be packaged into new virions (Flynn et al., 2022) (Figure 1). M^{pro} is one of two

cysteine proteases of SARS-CoV-2, and its active site consists of four pockets (S1', S1, S2, S3),

with the S1' pocket containing a catalytic dyad composed of Cys145 and His41 residues. The

cleavage of the viral polyproteins by M^{pro} typically involves a Leu-Gln(Ser-Ala-Gly) recognition

motif shared among coronaviruses (Citarella et al., 2021). The dimerization of M^{pro} is necessary

for the full enzymatic activity of the protein, as the dimerization interface connects to the active

site (Citarelli et al., 2021) (Figure 2).
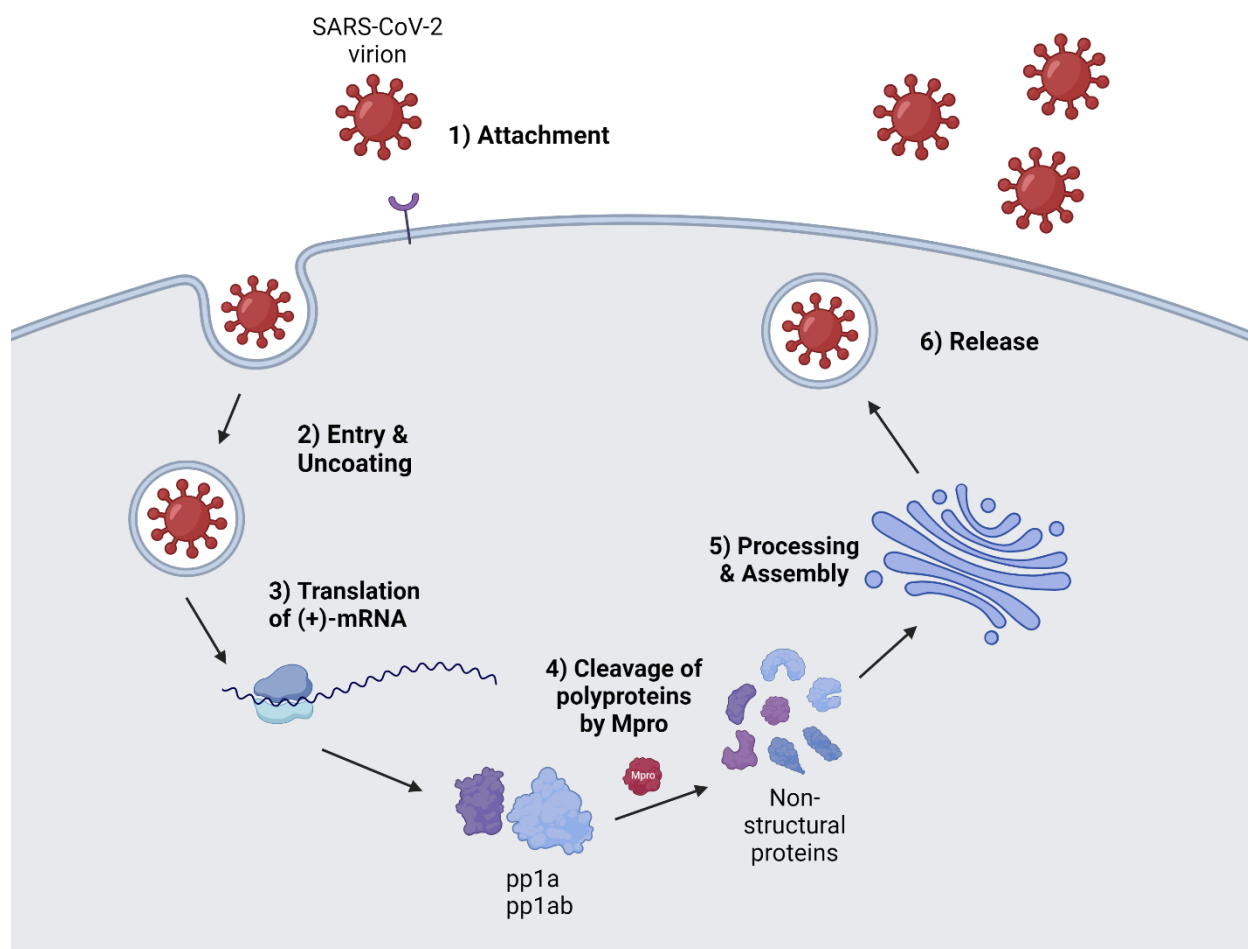
Figure 1. M^pro is essential in the replication cycle of SARS-CoV-2. After the translation of the positive-sense viral mRNA into the polyproteins 1a and 1ab, M^pro cleaves the polyproteins into the non-structural proteins. These form the replication complex to transcribe the sub-genomic RNA, which is then translated by host proteins. This results in the assembly and release of the mature virus. Figure created in BioRender.

The M^pro inhibitor in Paxlovid, nirmatrelvir, can covalently bind to the M^pro active site, thus blocking the protease from performing essential cleavages (Cho et al., 2023). Ritonavir is included in Paxlovid to improve the pharmacokinetic profile by inhibiting cytochrome P450 3A4 (CYP3A4), a human enzyme that metabolizes nirmatrelvir (Reis et al., 2022). However, many

reports of SARS-CoV-2 rebound after Paxlovid treatment indicate the serious possibility of the development of drug resistance in M^{pro} (Duan et al., 2023, Tamura et al., 2024).

(1) Active homodimeric form
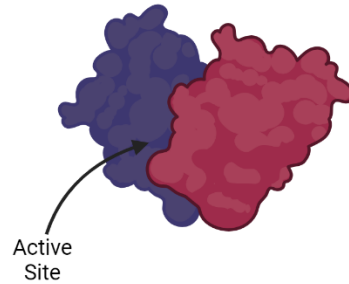
Active
Site

(2) Inactive monomeric form
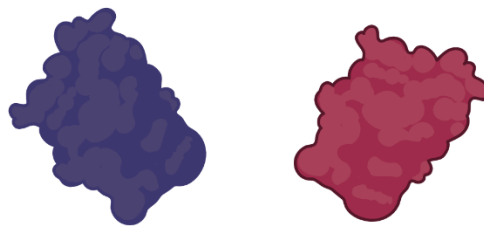
Figure 2. Dimerization of M^{pro} is necessary for its proteolytic activity. The M^{pro} active site is in a pocket adjacent to the dimeric interface. The monomeric form of M^{pro} does not have proteolytic activity. Figure created in BioRender.

Extensive antiviral drug exposure in combination with multiple viral replication cycles frequently result in antiviral drug resistance. In August 2023, the E166V mutation in M^{pro} was identified in a patient with severe COVID-19 who received repeated and prolonged treatment of Paxlovid (i.e., NIR) (Zuckerman et al., 2024). The E166V mutation had been previously shown to result in significant NIR resistance in passaging studies (Iketani et al., 2023, Zhou et al., 2022). Despite this, GC376, a protease inhibitor used against another coronavirus called feline infectious peritonitis virus (FIPV) known to also inhibit the SARS-CoV-2 M^{pro} (Hu et al., 2022,

Paciaroni et al., 2023, Wang et al., 2020), has been shown to still inhibit M^{pro} with the E166V mutation (Lan et al., 2023).

However, this mutation also results in decreased viral fitness (Zhou et al., 2022). The E166 residue is located in the M^{pro} S1 substrate-binding site and plays a critical role in dimer stabilization (Cheng et al., 2010, Tan et al., 2005). The E166 residue, alongside the F140 and H163 residues, form hydrogen bonds with a water molecule located in the active site, which stabilizes the oxyanion hole (Citarelli et al., 2021). Therefore, mutations in the E166 residue can lead to destabilization in the dimer and decreased enzyme activity as seen in SARS-CoV M^{pro} (Pillaiyar et al., 2016).

The stabilization of the architecture of the active site plays a crucial role in the maintenance of M^{pro} activity in SARS-CoV (Li et al., 2016). Residues Ser139-Phe140-Leu141 participate in maintaining the correct conformation of the S1 substrate-binding site in the active enzyme. The conformational flexibility of Leu141 favors the formation of a short 3_{10}-helix in the catalytic site of M^{pro} in the absence of interactions with the N-finger of Domain I and the E166 residue, which disrupts the catalytic machinery of M^{pro}. Changing Leu141 to a Thr, which favors the β-sheet secondary structure, allows for increased active site stability and increased enzymatic activity in SARS-CoV M^{pro} (Li et al., 2016). The M^{pro} of SARS-CoV is extremely similar to that of SARS-CoV-2, with 83% sequence identity and 3D structure similarity (Razali et al., 2021). Therefore, mutations in SARS-CoV M^{pro} should have similar effects for SARS-CoV-2 M^{pro}.

Previous research has been conducted in elucidating the mechanism behind the decreased fitness and NIR resistance from the E166V mutation (Duan et al., 2023, Hu et al., 2023, Iketani et al., 2023, Paciaroni et al., 2023, Tan et al., 2005, Zhou et al., 2022). Other studies have investigated

the effects of the E166V mutation in combination with other mutations (Goyal & Goyal, 2020, Iketani et al., 2023, Zhou et al., 2022), but none have specifically investigated the E166V + L141T mutant. In addition, the effects of the L141T mutation have only been studied for the SARS-CoV M^{pro} and have not been previously investigated for the SARS-CoV-2 M^{pro} (Li et al., 2016), and few studies have looked at dimerization for SARS-CoV-2 M^{pro} (Goyal & Goyal, 2020, Paciaroni et al., 2023).

In this study, I investigated the effect of L141T on both drug resistance and activity of SAR-CoV-2 M^{pro} and possible compensatory mechanisms. I hypothesize that the introduction of the L141T mutation would increase the dimerization and therefore the enzymatic activity of the Omicron (BA.1) resistant mutant E166V M^{pro} without decreasing NIR resistance or increasing GC376 resistance. Comparison of the L141T mutation in combination with the E166V mutation will allow me to isolate the effect the L141T mutation has on both fitness and drug resistance to NIR and GC376.

Materials & Methods

Protein Expression & Purification

Site-directed mutagenesis was used to introduce the L141T mutation into BA.1 WT and BA.1 E166V plasmids. BL21-DE3 *Escherichia coli* cells were transformed with the BA.1 L141T/E166V expression plasmids. The bacteria were grown in lysogeny broth (LB) at 37°C in the presence of carbenicillin and chloramphenicol until it reached an optical density (OD_{600}) of 0.8. Protein expression was induced using isopropyl ß-D-1-thiogalactopyranoside (IPTG). The bacterial cells were cooled to 18°C, and then let to grow overnight. Cells were lysed with sonication. The His-tagged proteins were purified from the lysate via a Ni^{2+} column. The His tag

was then cleaved using the human rhinovirus (HRV) 3C protease. Protein expression was verified using SDS-PAGE.

Kinetics Assay

A FRET (Förster Resonance Energy Transfer)-based activity assay was used to evaluate the activity of the of the BA.1 L141T/E166V M^{pro} by determining the Michaelis-Menten constant (K_m) and the catalytic constant (k_{cat}) against varying concentrations of a fluorescent substrate (MCA-AVLQSGFR-Lys(Dnp)-Lys-NH_2) (Figure 3). These two values were used to determine the specificity constant, which is equal to k_{cat}/K_m. This substrate peptide is a derivative of the SARS-CoV-2 M^{pro} N-terminal auto-processing site, whose cleavage by M^{pro} results in the release of a fluorescent 7-methoxycoumarin (MCA) moiety from a 2,4-dinitrophenol (Dnp) quenching agent (Ye et al., 2023). The resulting increase in fluorescent intensity was used as a proxy for enzymatic activity. 40 μM of the fluorescent substrate was serially diluted. A reverse dilution of DMSO was conducted to account for the inhibitory effects of DMSO on fluorescence. Bovine serum albumin (BSA) was used as a negative control to account for the fluorescent effects of tyrosine and tryptophan residues. Fluorescent intensity was monitored using BioTek Cytation 3 every 60 seconds for thirty minutes at room temperature upon the addition of the substrate to the protein. The L141T/E166V and E166V mutants were run at 2 μM, whereas the WT was run at 1 μM. The reaction was conducted in 20 mM Bis-Tris. Each assay included three technical replicates, and the kinetics constants were calculated based on three biological replicates.
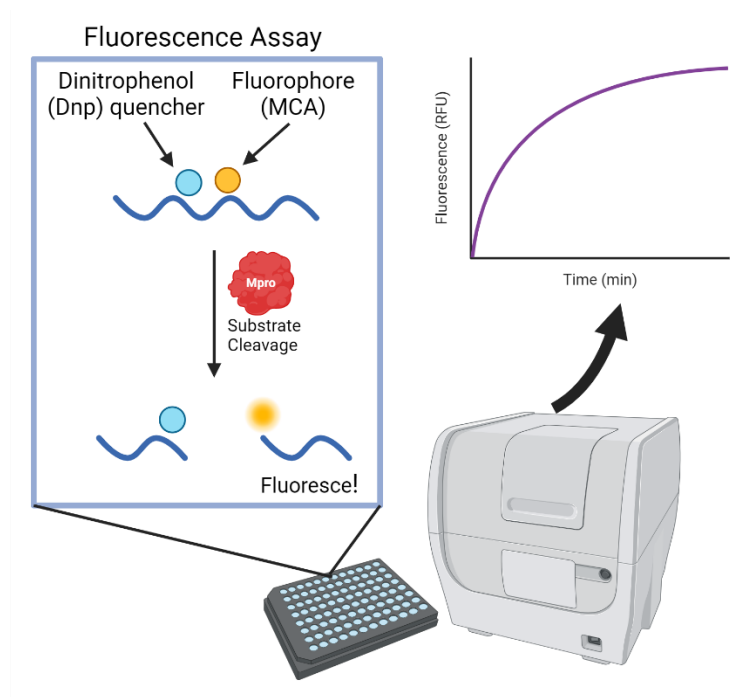
Figure 3. Fluorescence Assay. The un-cleaved substrate (MCA-AVLQSGFR-Lys(Dnp)-Lys-NH$_2$) contains a dinitrophenol (Dnp) quencher and a fluorescent 7-methoxycoumarin (MCA) moiety. The chemical cleavage of substrate by M^{pro} results in the release of Dnp from MCA. This results in an increase in fluorescent intensity, which was monitored using the BioTek Cytation 3 plate reader. The usage of fluorescent intensity as a measurement of enzymatic activity is utilized in both the kinetics assay and IC$_{50}$ assay. Figure created in BioRender.

Data analysis was conducted using Jupyter Lab (Figure 4). Linear regression was used to determine the slope and correlation coefficient (r) for each trial. The triplicate slopes were averaged for each substrate concentration. The Michaelis-Menten equation (Equation 1) was then used to determine the maximum velocity (V$_{max}$) and K$_m$. The catalytic constant k$_{cat}$ was calculated by dividing the V$_{max}$ by the enzyme concentration, and the specificity constant was determined by dividing the k$_{cat}$ by K$_m$.

$$V_i = \frac{V_{max} [S]}{K_m + [S]}$$

Equation 1. The Michaelis-Menten equation. [S] refers to the substrate concentration. V_{max} refers to the maximum reaction velocity, and K_m refers to the Michaelis-Menten constant, which is the concentration of substrate at half the maximum velocity.
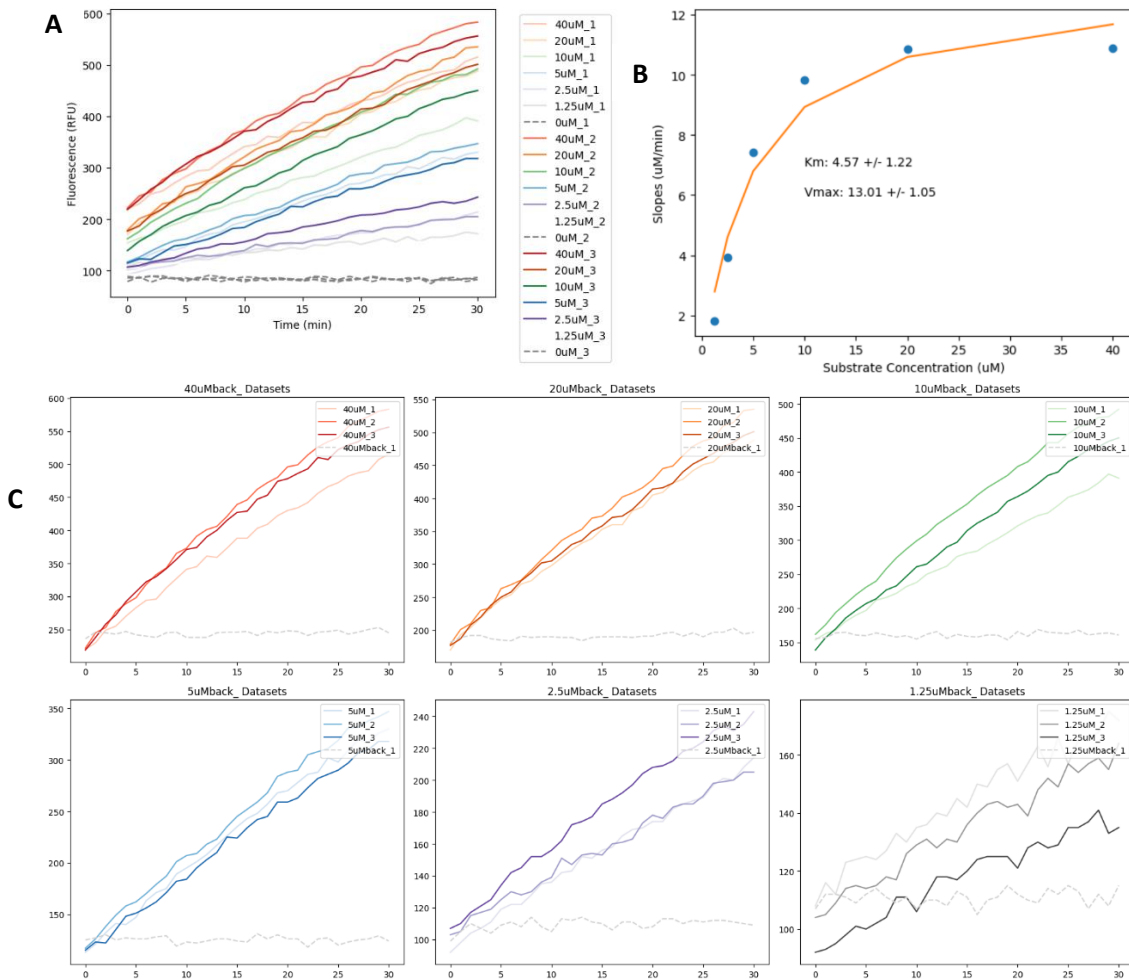
Figure 4. Representative kinetics assay results, analysis, and calculations for the cleavage of the fluorescent substrate by BA.1 L141T/E166V. Statistical analyses were conducted in Jupyter Lab. (A) The raw data values for the fluorescence values were graphed against the time.

The dashed lines represent the baseline enzyme fluorescence without the addition of substrate. (B) Linear regression was used to determine the slopes and R-values for each substrate concentration, which was then plotted against the substrate concentration. (C) The changes in fluorescence for the triplicates at each substrate concentration were graphed against time. The dashed line represents the fluorescence levels of the addition of Bovine Serum Albumin (BSA) to each concentration of substrate, normalized using the extinction coefficient.

IC50 Assay

The FRET-based assay was also used to characterize the efficacy of drug inhibition by determining the half-maximal inhibitory concentrations (IC_{50}) values for the inhibition of WT, E166V, and L141T/E166V M^{pro} cleavage of the fluorescent substrate by NIR and GC376 (Figure 3). FRET assays have been previously used to characterize the drug inhibition of SARS-CoV-2 M^{pro} (Narayanan et al., 2022, Wang et al., 2020). 200 μM NIR and 25 μM GC376 were serially diluted. A reverse dilution of DMSO was conducted to account for the inhibitory effects of DMSO on fluorescence, as the drugs are stored in DMSO. 2 μM of the L141T/E166V protein was added to both drugs and incubated at 37°C for 10 minutes. Fluorescent intensity was monitored every 90 seconds for thirty minutes at room temperature upon the addition of 50 μM substrate to the protein-drug solution. The reaction was conducted in 20 mM Bis-Tris. Each assay included three technical replicates, and the IC_{50} was calculated based on three biological replicates.

Data analysis was conducted using RStudio. The slope of the first four data points of the change in fluorescence at each drug concentration was determined (Figure 5A). The linearity of these first four points was checked to ensure that only the linear portion of the kinetic curve is used

9

(Figure 5B). The slopes were normalized to the no drug condition and then were graphed against the drug concentration. A sigmoidal curve was fitted to the data (Figure 5C). The IC_{50} value is equal to the concentration at the half-maximal response.
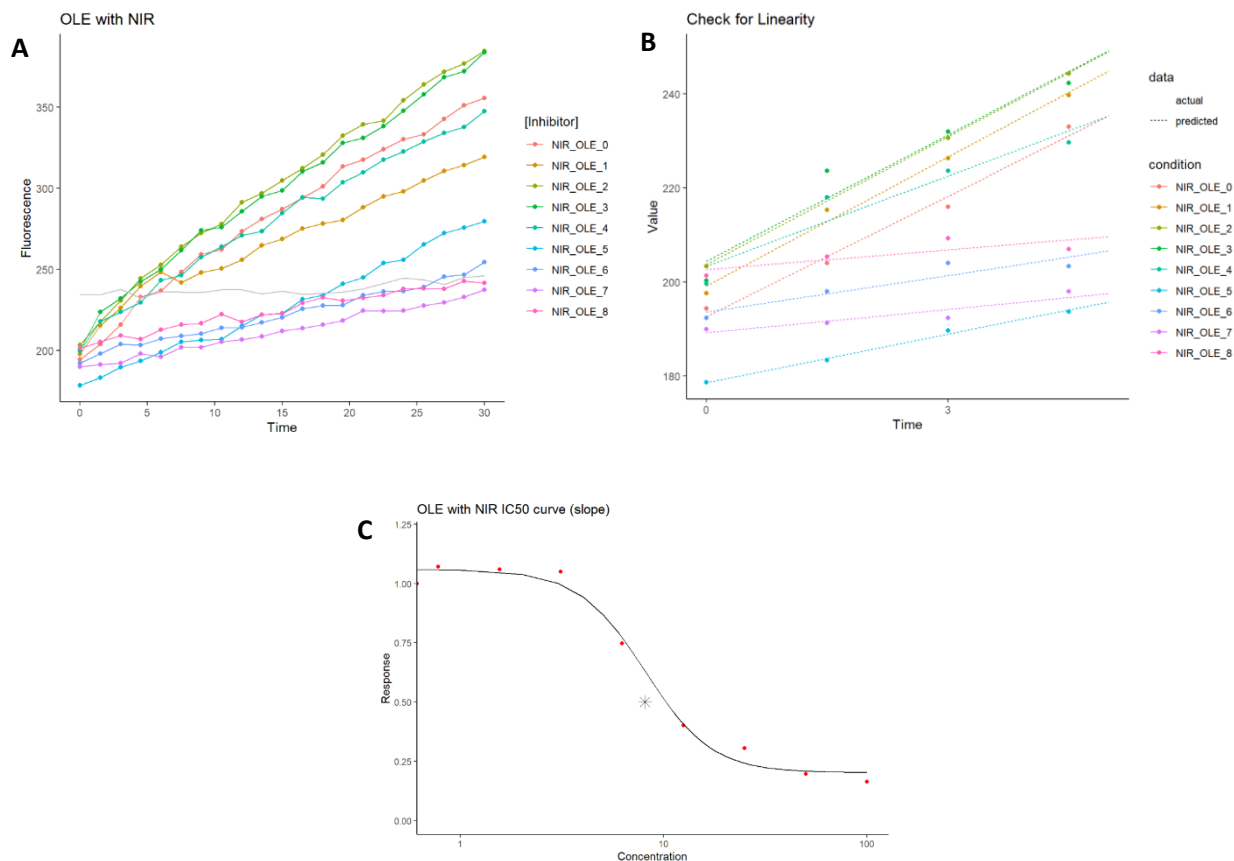
Figure 5. Representative FRET-based assay results, analysis, and IC50 calculation for inhibition of the BA.1 L141T/E166V (OLE) Mpro protein by Nirmatrelvir (NIR). Statistical analyses were conducted in RStudio. (A) The raw data values for the fluorescence values graphed against the time. NIR_OLE_0 represents the change in fluorescence without the addition of any inhibitor to the solution. The concentration of the drug increases twofold as we go from NIR_OLE_1 to NIR_OLE_8. (B) Linearity check of the first four data points for each concentration of Nirmatrelvir. (C) The slopes were scaled and then graphed against the

10

concentration of Nirmatrelvir. A sigmoidal curve was fitted. The star (*) represents the IC_{50} value, the concentration at which the half-maximal inhibitory activity occurs.

SEC-MALS

SEC-MALS (Size Exclusion Chromatography with Multi-Angle Light Scattering) was utilized to characterize the monomer-dimer equilibrium of the WT, E166V, and L141T/E166V M^{pro} proteins (Figure 6). Size-exclusion chromatography separates the components in solution by size, and multi-angle light scattering then characterizes the molecular weight of each component, thereby separating, identifying, and quantifying the amount of monomer and dimer in solution (Some et al., 2019). Comparing the relative proportions of M^{pro} monomer and dimer in solution was used to determine any effects on the dimerization equilibrium caused by E166V and L141T/E166V M^{pro}.

Solutions of 60 μM and 15 μM of the three mutants were run. 15 μM of enzyme was then run with 75 uM of GC376 and NIR. 2 mg/mL BSA was used as a control. Data collection and analysis was conducted using Wyatt Technologies Dawn Heleos II.
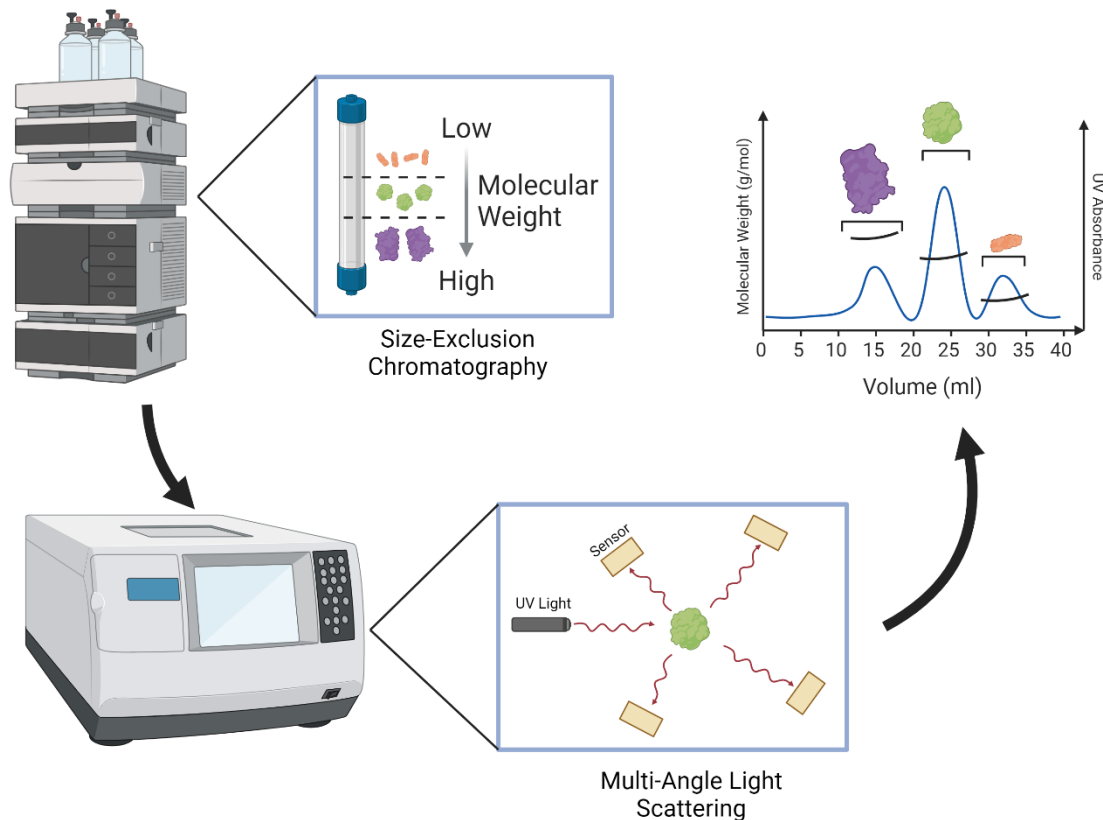
Figure 6. Size Exclusion Chromatography Multi-Angle Light Scattering. Proteins in solution are first separated by molecular weight using size exclusion chromatography. Ultraviolet light is shined onto the protein, and the refractive indexes of the scattered light were used to determine the volume of the protein. The average density of proteins and the volume was then used to determine the absolute molecular weight of the protein components in solution. Figure created in BioRender.

Results

The L141T mutation decreases proteolytic activity of the BA.1 E166V M^{pro}. The specificity constant is the highest for the WT, indicating that the WT enzyme has the highest efficiency of substrate cleavage (Table 1). This efficiency drastically decreases with the E166V construct,

reflecting the decreased viral fitness due to dimer destabilization. The introduction of the L141T

mutation to the E166V protein slightly decreases the specificity constant, indicating that the

double mutant L141T/E166V is the least efficient in proteolytic cleavage of the three mutants.

The K_m, which also serves as a measure of the binding affinity of the enzyme for its substrate,

indicates that the WT has the greatest binding affinity, whereas the E166V and the

L141T/E166V have similar binding affinities.

Table 1. Kinetics Parameters for BA.1 M^{pro} Mutants

	BA.1 Wildtype (1 μM)	BA.1 E166V (2 μM)	BA.1 L141T/E166V (2 μM)
K_m (μM)	2.83 ± 0.8	4.76 ± 1.0	4.52 ± 0.7
V_{max} (μM/min)	23.4 ± 2.1	23.5 ± 2.7	12.1 ± 0.6
Specificity Constant ($\mu M^{-1}min^{-1}$)	9.67 ± 3.0	2.56 ± 0.7	1.34 ± 0.2

The L141T/E166V construct still demonstrates significant NIR resistance. The low IC_{50}

value for the inhibition of the BA.1 WT M^{pro} by NIR indicates that NIR is most effective at

inhibiting the WT enzyme (Table 2). The E166V mutant demonstrates high NIR resistance. The

IC_{50} value for the inhibition of the L141T/E166V M^{pro} by NIR is significantly higher than that

for the WT M^{pro}, indicating that the L141T/E166V mutant enzyme demonstrates NIR resistance.

However, the introduction of the L141T mutation results in decreased NIR resistance compared

to the E166V mutant.

There is no significant difference in IC_{50} values for the inhibition of the BA.1 WT and E166V

M^{pro} by GC376, indicating that the E166V mutation does not affect inhibition by GC376, as the

E166V mutation is only NIR resistant. We do observe a slight decrease in IC_{50} upon the introduction of the L141T mutation to the E166V protein, meaning that the L141T/E166V is remains susceptible to inhibition by GC376.

Table 2. IC_{50} Values for the Inhibition of BA.1 M^{pro} Mutants by Nirmatrelvir and GC376 (μM ± SD)

	BA.1 Wildtype	BA.1 E166V	BA.1 L141T/E166V
Nirmatrelvir	0.778 ± 0.06	26.5 ± 18	9.19 ± 1.3
GC376	1.13 ± 0.1	1.27 ± 1.6	0.653 ± 0.050

The L141T mutation partially rescues the dimerization lost from the E166V mutation. The SEC-MALS allows us to investigate the effects of mutations on the monomer-dimer equilibrium of M^{pro} in solution. BA.1 WT reveals a strong peak for the dimer, with a smaller but noticeable peak for the monomer (Figure 7, top row). In contrast, a broad band is observed for BA.1 E166V, indicating a mixed population where most of the protein is in its monomeric form and a small amount of dimer in solution that is not significant enough to result in a distinct peak. In contrast, there are two distinct peaks for the BA.1 L141T/E166V, with a significantly higher proportion of dimer than monomer in solution. However, the dimerization of L141T/E166V is less than the dimerization of the WT, meaning that the L141T/E166V only partially restored the dimerization lost due to the E166V mutation.

Due to Le Chatelier's principle, lowering the concentration of all three mutants results in a higher proportion of monomer in solution. At the decreased concentration, there is still a significant dimer peak for the WT construct, whereas the E166V construct only shows a

monomer peak. In contrast to the E166V, the L141T/E166V reveals two distinct peaks, with a slightly higher proportion of monomer than dimer in solution.

The addition of NIR and GC376 to all three mutants results in a shift towards dimerization due to substrate-induced dimerization (Figure 7, bottom row). GC376 resulted in a stronger induced dimerization than NIR for the E166V and L141T/E166V constructs, whereas the two drugs had similar effects on the WT. This difference is likely due to difference in how the drugs bind to, and thus stabilize, the active site. Specifically, the addition of NIR to the E166V construct results in a broad band at the monomer peak, meaning that the concentration of dimer is too low to result in a separate peak, whereas GC376 results in a strong dimeric peak. In contrast, the addition of NIR to the L141T/E166V construct results in two distinct peaks, with a higher proportion of monomer than dimer in solution. This data is consistent with the IC_{50} experiments indicating that the L141T/E166V demonstrates some resistance to NIR but not as high as E166V alone.
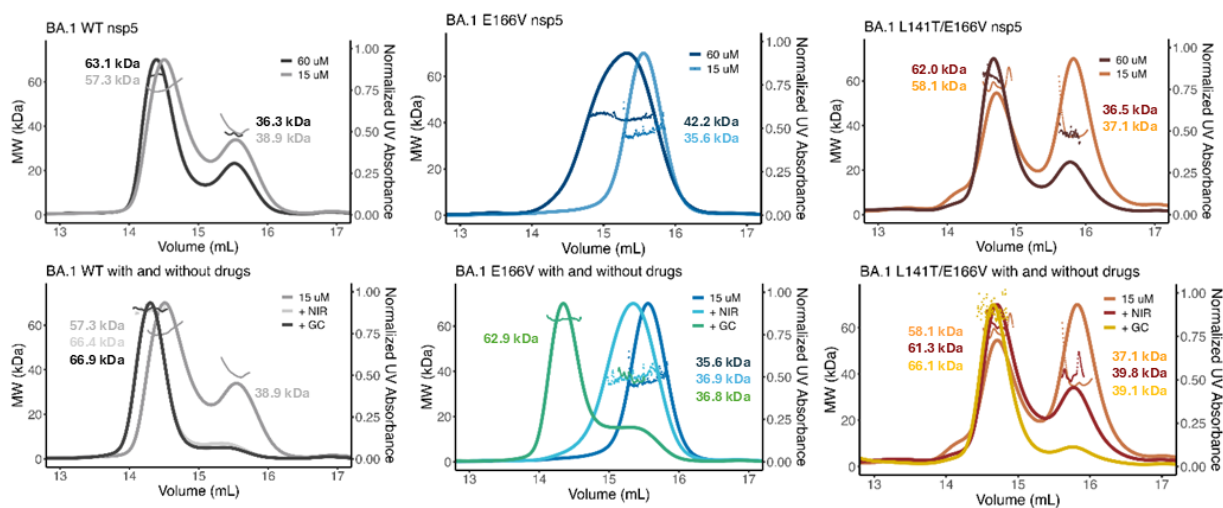
Figure 7. SEC-MALS experiments reveal the monomer-dimer equilibrium of the BA.1 M^{pro} mutants in solution. The right peak represents the monomeric form, and the left peak represents

the dimeric form. Broad bands indicate mixtures of monomers and dimers. (Top row) The BA.1

L141T/E166V M^{pro} shows a significantly higher proportion of dimers compared to the BA.1

E166V. Decreasing the concentration of all three mutants of M^{pro} results in a shift towards the

monomeric form. (Bottom row) The BA.1 L141T/E166V M^{pro} shifts towards dimerization upon

the addition of M^{pro} inhibitors. When nirmatrelvir (NIR) is added, the higher proportion of

monomerization of the L141T/E166V compared to the WT indicates that the L141T/E166V has

nirmatrelvir resistance.

Table 3. Calculated molecular weight (MW) and percent mass (Mass %) from SEC-MALS.

	Dimer peak		Monomer peak	
	MW / kDa	**Mass %**	**MW / kDa**	**Mass %**
WT-nsp5$_{BA.1}$ (60 μM)	63.1 ($\pm < 0.1\%$)	71.7	36.3 ($\pm 0.2\%$)	28.3
WT-nsp5$_{BA.1}$ (15 μM)	57.3 ($\pm 0.1\%$)	70.5	38.9 ($\pm 0.3\%$)	29.5
WT-nsp5$_{BA.1}$ + NIR	66.4 ($\pm 0.1\%$)	100	N/A	N/A
WT-nsp5$_{BA.1}$ + GC	66.9 ($\pm 0.1\%$)	100	N/A	N/A
E166V-nsp5$_{BA.1}$ (60 μM)	N/A	N/A	42.2 ($\pm 0.2\%$)	100
E166V-nsp5$_{BA.1}$ (15 μM)	N/A	N/A	35.6 ($\pm 0.3\%$)	100
E166V-nsp5$_{BA.1}$ + NIR	N/A	N/A	36.9 ($\pm 0.2\%$)	100
E166V-nsp5$_{BA.1}$ + GC	62.9 ($\pm 0.1\%$)	83.1	36.8 ($\pm 0.3\%$)	16.9
L141T/E166V-nsp5$_{BA.1}$ (60 μM)	62.0 ($\pm 0.4\%$)	71.8	36.5 ($\pm 0.8\%$)	28.2
L141T/E166V-nsp5$_{BA.1}$ (15 μM)	58.1 ($\pm 0.7\%$)	43.9	37.1 (± 0.7)	56.1
L141T/E166V-nsp5$_{BA.1}$ + NIR	61.3 ($\pm 0.4\%$)	43.9	39.8 ($\pm 1.0\%$)	34.7
L141T/E166V-nsp5$_{BA.1}$ + GC	66.1 ($\pm 0.8\%$)	90.8	39.1 ($\pm 5.4\%$)	8.2

**The MW and Mass % of each peak are shown in instances where distinct monomer and dimer

peaks were observed.

Discussion:

Overall, this project investigated the effects of the L141T mutation on the NIR-resistant BA.1 E166V M^{pro}. The L141T/E166V mutant has decreased proteolytic efficiency compared to both the WT and E166V mutants and demonstrates intermediate NIR resistance. Such NIR resistance was also demonstrated in the decreased dimerization of the L141T/E166V M^{pro} in the presence of NIR compared to GC376. Similar to the other mutants, the L141T/E166V M^{pro} demonstrated substrate-induced dimerization in the presence of the M^{pro} inhibitors.

Despite the increased dimerization of the L141T/E166V M^{pro} compared to the E166V M^{pro}, as observed in the SEC-MALS experiments, the L141T/E166V shows decreased enzymatic activity. These results are surprising, as it is normally expected that increased dimerization results in increased proteolytic cleavage. However, we may have not accounted for the fact that the structural changes introduced in the L141T mutation may have decreased the affinity for the fluorescent substrate by changing the architecture or electrostatic potential of the S1 pocket.

For the relatively inactive E166V mutant, I noticed that in the kinetics experiments, the addition of high concentrations of substrate resulted in a decreased reaction velocity, as opposed to approaching a maximum velocity as seen in typical Michaelis-Menten kinetics (Figure 8). This pattern reflects a phenomenon known as substrate inhibition, in which excess substrate has an inhibitory effect on enzymatic activity (Reed et al., 2010). Approximately 20% of enzymes demonstrate this phenomenon, although this has not been commonly observed in chymotrypsin-like proteases such as M^{pro} (Reed et al., 2010).
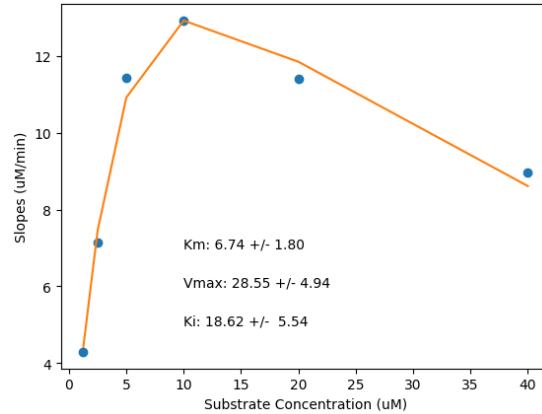
Figure 8. The BA.1 E166V demonstrates substrate inhibition. The kinetics experiments reveal a deviation from typical Michaelis-Menten kinetics, where instead of approaching a maximum velocity, higher concentrations of substrate results in decreased velocity.

For the E166V protein, the K_m and V_{max} were recalculated by introducing a third variable into the Michaelis-Menten equation: the substrate inhibition constant K_i (Equation 2). By including the K_i, we noticed that the calculated K_m and V_{max} are much higher than the values calculated with the original Michaelis-Menten equation. The recalculated values are included in Table 1.

$$V_i = \frac{V_{max}\,[S]}{K_m + [S] + \left(\frac{[S]^2}{K_i}\right)}$$

Equation 2. The modified Michaelis-Menten equation incorporating the substrate inhibition constant K_i.

This study demonstrated that improving the dimerization of M^{pro} does not necessarily improve its fitness. However, these experiments were conducted *in vitro*, and there is a possibility that enzymatic behavior may change in an *in vivo* system such as cell culture or animal models. These experiments also do not clarify how the L141T specifically changes the M^{pro} active site

18

and dimerization interface. Further experiments such as X-ray crystallography may elucidate the specific interactions of the L141T mutation with the M^{pro} active site including the N-terminus of the opposite protomer, as well as how L141T affects the protein-drug interactions of NIR and GC376.

Coronaviruses such as MERS, SARS-CoV, and SARS-CoV-2 have caused devastating effects in the past, and it is not unlikely that the next major epidemic would be caused by a coronavirus. Given the rapid mutation rate of coronaviruses and other ssRNA viruses, it is important to anticipate any potential drug-resistance mutations to ensure that there is no over-reliance on a single antiviral drug. Understanding not only how resistance develops but compensatory mutations that improve activity provides crucial information for designing future inhibitors. Although the rate of COVID-19 cases has dramatically decreased since 2024, SARS-CoV-2 still has not been eradicated as of 2024, and antiviral drugs for SARS-CoV-2 are still under development.

References:

Cheng, Shu-Chun, et al. "Mutation of Glu-166 Blocks the Substrate-Induced Dimerization of SARS Coronavirus Main Protease." Biophysical Journal, vol. 98, no. 7, Apr. 2010, pp. 1327–36. PubMed Central, https://doi.org/10.1016/j.bpj.2009.12.4272.

Cho, Junhyung, et al. "Evaluation of Antiviral Drugs against Newly Emerged SARS-CoV-2 Omicron Subvariants." Antiviral Research, vol. 214, June 2023, p. 105609. PubMed, https://doi.org/10.1016/j.antiviral.2023.105609.

Citarella, Andrea, et al. "SARS-CoV-2 Mpro: A Potential Target for Peptidomimetics and Small-

> Molecule Inhibitors." Biomolecules, vol. 11, no. 4, Apr. 2021, p. 607. PubMed Central,

> https://doi.org/10.3390/biom11040607.

"COVID-19 Cases | WHO COVID-19 Dashboard." Datadot,

> https://data.who.int/dashboards/covid19/cases. Accessed 14 Mar. 2024.

COVID-19 Treatments | NIH COVID-19 Research. 27 Sept. 2023,

> https://covid19.nih.gov/covid-19-treatments.

Duan, Yinkai, et al. "Molecular Mechanisms of SARS-CoV-2 Resistance to Nirmatrelvir."

> Nature, vol. 622, no. 7982, Oct. 2023, pp. 376–82. PubMed,

> https://doi.org/10.1038/s41586-023-06609-0.

Flynn, Julia M., et al. "Comprehensive Fitness Landscape of SARS-CoV-2 Mpro Reveals

> Insights into Viral Resistance Mechanisms." eLife, vol. 11, June 2022, p. e77433.

> PubMed Central, https://doi.org/10.7554/eLife.77433.

Goyal, Bhupesh, and Deepti Goyal. "Targeting the Dimerization of the Main Protease of

> Coronaviruses: A Potential Broad-Spectrum Therapeutic Strategy." ACS Combinatorial

> Science, vol. 22, no. 6, June 2020, pp. 297–305. ACS Publications,

> https://doi.org/10.1021/acscombsci.0c00058.

Hu, Ben, et al. "Characteristics of SARS-CoV-2 and COVID-19." Nature Reviews

> Microbiology, vol. 19, no. 3, Mar. 2021, pp. 141–54. www.nature.com,

> https://doi.org/10.1038/s41579-020-00459-7.

Hu, Yanmei, et al. "Naturally Occurring Mutations of SARS-CoV-2 Main Protease Confer Drug

    Resistance to Nirmatrelvir." ACS Central Science, vol. 9, no. 8, July 2023, pp. 1658–69.

    PubMed Central, https://doi.org/10.1021/acscentsci.3c00538.

Iketani, Sho, et al. "Multiple Pathways for SARS-CoV-2 Resistance to Nirmatrelvir." Nature,

    vol. 613, no. 7944, 2023, pp. 558–64. PubMed Central, https://doi.org/10.1038/s41586-

    022-05514-2.

Lan, Shuiyun, et al. Nirmatrelvir Resistance in SARS-CoV-2 Omicron_BA.1 and WA1

    Replicons and Escape Strategies. bioRxiv, 3 Jan. 2023, p. 2022.12.31.522389. bioRxiv,

    https://doi.org/10.1101/2022.12.31.522389.

Li, Chunmei, et al. "Conformational Flexibility of a Short Loop near the Active Site of the

    SARS-3CLpro Is Essential to Maintain Catalytic Activity." Scientific Reports, vol. 6, no.

    1, 1, Feb. 2016, p. 20918. www.nature.com, https://doi.org/10.1038/srep20918.

Narayanan, Anoop, et al. "Identification of SARS-CoV-2 Inhibitors Targeting Mpro and PLpro

    Using in-Cell-Protease Assay." Communications Biology, vol. 5, no. 1, 1, Feb. 2022, pp.

    1–17. www.nature.com, https://doi.org/10.1038/s42003-022-03090-9.

Paciaroni, Alessandro, et al. "Stabilization of the Dimeric State of SARS-CoV-2 Main Protease

    by GC376 and Nirmatrelvir." International Journal of Molecular Sciences, vol. 24, no. 7,

    Mar. 2023, p. 6062. PubMed Central, https://doi.org/10.3390/ijms24076062.

Pillaiyar, Thanigaimalai, et al. "An Overview of Severe Acute Respiratory Syndrome–

    Coronavirus (SARS-CoV) 3CL Protease Inhibitors: Peptidomimetics and Small Molecule

Chemotherapy." *Journal of Medicinal Chemistry*, vol. 59, no. 14, July 2016, pp. 6595–628. *ACS Publications*, https://doi.org/10.1021/acs.jmedchem.5b01461.

Razali, Rafida, et al. "Structure-Function Characteristics of SARS-CoV-2 Proteases and Their Potential Inhibitors from Microbial Sources." Microorganisms, vol. 9, no. 12, Nov. 2021, p. 2481. PubMed Central, https://doi.org/10.3390/microorganisms9122481.

Reed, Michael C., et al. "The Biological Significance of Substrate Inhibition: A Mechanism with Diverse Functions." *BioEssays*, vol. 32, no. 5, 2010, pp. 422–29. *Wiley Online Library*, https://doi.org/10.1002/bies.200900167.

Reis, Stefanie, et al. "Nirmatrelvir Combined with Ritonavir for Preventing and Treating COVID-19." The Cochrane Database of Systematic Reviews, vol. 2022, no. 9, Sept. 2022, p. CD015395. PubMed Central, https://doi.org/10.1002/14651858.CD015395.pub2.

Some, Daniel, et al. "Characterization of Proteins by Size-Exclusion Chromatography Coupled to Multi-Angle Light Scattering (SEC-MALS)." Journal of Visualized Experiments: JoVE, no. 148, June 2019. PubMed, https://doi.org/10.3791/59615.

Tamura, Trevor J., et al. "Emerging SARS-CoV-2 Resistance After Antiviral Treatment." *JAMA Network Open*, vol. 7, no. 9, Sept. 2024, p. e2435431. *Silverchair*, https://doi.org/10.1001/jamanetworkopen.2024.35431.

Tan, Jinzhi, et al. "pH-Dependent Conformational Flexibility of the SARS-CoV Main Proteinase (Mpro) Dimer: Molecular Dynamics Simulations and Multiple X-Ray Structure

Analyses." Journal of Molecular Biology, vol. 354, no. 1, Nov. 2005, pp. 25–40. PubMed

Central, https://doi.org/10.1016/j.jmb.2005.09.012.

V'kovski, Philip, et al. "Coronavirus Biology and Replication: Implications for SARS-CoV-2."

Nature Reviews Microbiology, vol. 19, no. 3, Mar. 2021, pp. 155–70. www.nature.com,

https://doi.org/10.1038/s41579-020-00468-6.

Wang, Yu-Chuan, et al. "Structural Basis of SARS-CoV-2 Main Protease Inhibition by a Broad-

Spectrum Anti-Coronaviral Drug." American Journal of Cancer Research, vol. 10, no. 8,

Aug. 2020, pp. 2535–45.

Ye, Xin, et al. "Synthesis and Enzymatic Inhibition Effects of Thiazolidinedione 3C-like

Protease Inhibitors." Journal of Chemical Research, vol. 47, no. 1, Jan. 2023, p.

17475198231152556. SAGE Journals, https://doi.org/10.1177/17475198231152556.

Zhou, Yuyong, et al. "Nirmatrelvir-Resistant SARS-CoV-2 Variants with High Fitness in an

Infectious Cell Culture System." Science Advances, vol. 8, no. 51, 2022, p. eadd7197.

PubMed Central, https://doi.org/10.1126/sciadv.add7197.

Zuckerman, Neta S., et al. "Nirmatrelvir Resistance—de Novo E166V/L50V Mutations in an

Immunocompromised Patient Treated With Prolonged Nirmatrelvir/Ritonavir

Monotherapy Leading to Clinical and Virological Treatment Failure—a Case Report."

Clinical Infectious Diseases, vol. 78, no. 2, Feb. 2024, pp. 352–55. Silverchair,

https://doi.org/10.1093/cid/ciad494.